A Novel Multitaper Reassignment Method for Estimation of Phase Synchrony

Maria Sandsten
Centre for Mathematical Sciences
Lund University
Lund, Sweden
maria.sandsten@matstat.lu.se

Rachele Anderson
Centre for Mathematical Sciences
Lund University
Lund, Sweden
rachele.anderson@matstat.lu.se

Isabella Reinhold
Centre for Mathematical Sciences
Lund University
Lund, Sweden
isabella.reinhold@matstat.lu.se

Bo Bernhardsson
Dept of Automatic Control
Lund University
Lund, Sweden
bo.bernhardsson@control.lth.se

Carolina Bergeling
Dept of Automatic Control
Lund University
Lund, Sweden
carolina.bergeling@control.lth.se

Mikael Johansson
Dept of Psychology
Lund University
Lund, Sweden
mikael.johansson@psy.lu.se

***Abstract*—The matched phase reassignment, developed to estimate phase synchrony of transient oscillatory signals, is extended into a multitaper phase reassignment (MTPR) method. The method gives perfect time-frequency localization for two transients with zero phase difference and estimates of time locations and oscillatory frequencies in low signal-to-noise ratios. For different signal-to-noise ratios between channels a suggestion of corrected reassignment vector expressions is given, resulting in minimized variance. The MTPR outperforms the matched phase reassignment as well as state-of-the-art methods, such as Pearson's linear correlation, time-frequency cross-spectrogram phase estimation and the Phase Lag Index method. An example of estimated phase differences, time locations and oscillatory frequencies of electrical signals measured from the brain is also shown.**

***Index Terms*—time-frequency reassignment, oscillatory transient signals, phase synchronization, multitapers, EEG**

I. Introduction

For the past decades, functional neuroimaging techniques have produced impressive advances in knowledge of how the brain mediates cognition and behavior. Recent analysis developments leveraging machine learning have further shown that it is possible to accurately decode the content of mental representations based on brain activity [1]. For example, magnetic resonance imaging (fMRI) data may be used to classify semantic concepts [2]. However, in many cases, fMRI cannot capture the relevant activity, and Electroencephalography (EEG) is better suited to reveal the temporal dynamics of neural activity [3]–[5]. Scalp-recorded EEG signals have low signal-to-noise ratio (SNR), and methods robust to such disturbances are much needed.

Often important information is found from the spatial location of sources in the brain. To model the stream of information processing underlying mental states and extract features for reliable classification, both the brain signal's spatial and temporal dynamics need to be extracted [6], [7]. Further, with the attempt to actually capture the temporal dynamics, state-of-the-art methods simultaneously expand the signal into time and frequency, resulting in time-frequency (TF) representations. However, the underlying general methods of TF spectra are not optimally designed for resolving frequencies with temporal dynamics and important information is often hidden. The main drawback of commonly applied spectrograms is the limited TF resolution, which is known to cause spectral leakage and hidden information [8].

The reassignment technique is among the more popular methods today for TF visualization of oscillatory information [9]. For transient oscillatory signals we have invented a novel method, the matched reassigned spectrogram for estimation of the instantaneous time and frequency locations in the TF plane [10]–[13]. In [14], the matched reassigned spectrogram is expanded into a novel matched phase reassignment (MPR) method based on the reassigned cross-spectrogram. It is shown that for two phase synchronized oscillating transient signals, the method gives perfect TF localization. For low SNRs, degradation of the TF location estimates is seen, caused by the reassignment vectors being sensitive to noise, [12].

Multitapers are used to reduce variance of spectra, and the Hermite functions are the optimal choice with respect to TF resolution and orthogonality in the TF domain [15]. In [16] we presented a multitaper reassignment method, shown to give a high precision in the time- and frequency estimates in low SNR. In this paper we expand into a multitaper phase reassignment (MTPR) method for measurement of phase synchronization of two oscillatory transient signals.

The paper is outlined with preliminaries of the matched reassigned spectrogram in section 2, followed by a short overview of the multitaper reassignment in section 3. In section 4, the novel MTPR technique is proposed together with a suggestion for increased performance when SNR is differing between channels. The novel phase estimator is evaluated and

This work was supported by the Wallenberg Autonomous Systems and Software Program (WASP) funded by Knut and Alice Wallenberg Foundation.

compared to state-of-the-art estimators in section 5 and in section 6 an example of phase estimates from short transient oscillatory responses in EEG signals are shown. Conclusions are presented in section 7.

II. Preliminaries

Given a signal $x(t)$ the short-time Fourier transform (STFT) using the window $h(t)$ is

$$F_x^h(t,\omega) = \int_{-\infty}^{\infty} x(s)h^*(s-t)e^{-i\omega s}ds, \quad (1)$$

where * is the complex conjugate. The corresponding spectrogram is found as

$$S_x^h(t,\omega) = |F_x^h(t,\omega)|^2. \quad (2)$$

The reassigned spectrogram, where the spectrogram values are relocated to the corresponding $\hat{t}_x$ and $\hat{\omega}_x$ is defined as

$$RS_x^h(t,\omega) = \iint_{-\infty}^{\infty} S_x^h(s,\xi)\delta(t-\hat{t}_x(s,\xi),\omega-\hat{\omega}_x(s,\xi))ds\frac{d\xi}{2\pi} \quad (3)$$

with $\iint_{-\infty}^{\infty} f(t,\omega)\delta(t-t_0,\omega-\omega_0)dtd\omega/2\pi = f(t_0,\omega_0)$. In [10], the scaled reassigned spectrogram was proposed for which the reassignment vectors are computed with scaling constants $c_t,\ c_\omega$ as

$$\hat{t}_x^h(t,\omega) = t + c_t\Re\left(\frac{F_x^{th}(t,\omega)}{F_x^h(t,\omega)}\right) \quad (4)$$

$$\hat{\omega}_x^h(t,\omega) = \omega - c_\omega\Im\left(\frac{F_x^{\frac{dh}{dt}}(t,\omega)}{F_x^h(t,\omega)}\right) \quad (5)$$

where $\Re(\bullet)$ and $\Im(\bullet)$ represent the real and imaginary parts, and $F_x^{th}(t,\omega)$,$F_x^{\frac{dh}{dt}}(t,\omega)$ are the STFTs of the signal $x(t)$, with $t\cdot h(t)$ and $dh(t)/dt$ as window functions. In [10], this method was shown to have perfect time-frequency localization for estimation of Gaussian functions, which will be described in the following section. For the original reassignment technique, $c_t = c_\omega = 1$ [9].

III. The Multitaper Reassigned Spectrogram

The novel multitaper phase reassignment proposed in the following section stems from earlier works by the authors on multitaper reassignment of spectrograms. The latter will now be presented. Consider the oscillatory transient signal

$$x(t) = a(t-t_0)e^{-i\omega_0 t} \quad (6)$$

with a Gaussian envelope

$$a(t) = \frac{1}{\sqrt{\sigma\sqrt{\pi}}}e^{-t^2/(2\sigma^2)}. \quad (7)$$

In the matched window case $h(t) = a(-t)$, the scaled reassignment (4)-(5) with $c_t = c_\omega = 2$, reassigns all signal energy to $\hat{t}_x^h(t,\omega) = t_0$, and $\hat{\omega}_x^h(t,\omega) = \omega_0$ [10]. To achieve the TF localized reassignment for the second Hermite function window

$$h_2(t) = \frac{\sqrt{2}}{\sqrt{\sigma^3\sqrt{\pi}}}te^{-t^2/(2\sigma^2)} \quad (8)$$

orthogonal to $h(t) = a(-t)$, we proposed in [16] that the reassignment vector (4) is replaced by

$$\hat{t}_x^{h_2}(t,\omega) = t + d_t\Re\left(\frac{F_x^{th_2}(t,\omega)}{F_x^{h_2}(t,\omega)} - \sigma^2\frac{F_x^{\frac{dh_2}{dt}}(t,\omega)}{F_x^{h_2}(t,\omega)}\right) \quad (9)$$

and with $d_t = 1$, all signal energy is reassigned to $\hat{t}_x^{h_2}(t,\omega) = t_0$. Similarly, (5) is replaced by

$$\hat{\omega}_x^{h_2}(t,\omega) = \omega - d_\omega\Im\left(\frac{F_x^{\frac{dh_2}{dt}}(t,\omega)}{F_x^{h_2}(t,\omega)} - \frac{1}{\sigma^2}\frac{F_x^{th_2}(t,\omega)}{F_x^{h_2}(t,\omega)}\right) \quad (10)$$

and with $d_\omega = 1$, all signal energy is reassigned to $\hat{\omega}_x^{h_2}(t,\omega) = \omega_0$ [16]. Further, a multitaper reassigned spectrogram is proposed in [16] that average the reassignment vectors of the matched and non-matched reassigned spectrograms described above. In the following section, this idea will be applied to phase reassignment.

IV. The Multitaper Phase Reassignment

The matched phase reassignment [14], is a TF local measure of phase synchronization, where we define pairs of oscillatory transients with different amplitudes and phases as

$$y_n(t) = A_n x(t)e^{-i\phi_n} + e_n(t) \quad n = 1,2 \quad (11)$$

where $n = 1,2$ are two separate channels, $x(t)$ is defined as in (6) and the noise terms e_1 and e_2 also might have different variances, denoted s_1^2 and s_2^2. The corresponding cross-spectrogram is

$$S_{y_{1,2}}^h(t,\omega) = F_{y_1}^h(t,\omega)(F_{y_2}^h(t,\omega))^* \quad (12)$$

and the reassigned cross-spectrogram is found by replacing $S_x^h(t,\omega)$ with the absolute value $|S_{y_{1,2}}^h(t,\omega)|$ in (3). In [14] we suggested the following novel expressions as reassignment vectors,

$$\hat{t}_{y_{1,2}}^h = t + c_t\Re\left(\frac{F_{y_1}^{th}}{F_{y_2}^h} + \frac{F_{y_2}^{th}}{F_{y_1}^h}\right) \quad (13)$$

$$\hat{\omega}_{y_{1,2}}^h = \omega - c_\omega\Im\left(\frac{F_{y_1}^{\frac{dh}{dt}}}{F_{y_2}^h} + \frac{F_{y_2}^{\frac{dh}{dt}}}{F_{y_1}^h}\right) \quad (14)$$

where we have dropped (t,ω) in the expressions for convenience. The scaling factors c_t and c_ω are amplitude adjusted according to

$$c_t = c_\omega = 2\frac{A_1A_2}{A_1^2 + A_2^2}. \quad (15)$$

When $\phi_1 = \phi_2$, i.e. phase synchronization, (13,14) reduce to (4,5) with perfect TF localization to $\hat{t}_{y_{1,2}}^{h_1}(t,\omega) = t_0$ and $\hat{\omega}_{y_{1,2}}^{h_1}(t,\omega) = \omega_0$ if $h(t) = a(-t)$ [14].

In the case that the variances of the noise signals e_n in Eq. (11) differ and can be estimated, we propose the following alternative reassignment

$$\hat{t}^{h}_{y_{1,2}} = t + \Re\left(c_{t,1}\frac{F^{th}_{y_1}}{F^{h}_{y_2}} + c_{t,2}\frac{F^{th}_{y_2}}{F^{h}_{y_1}}\right), \tag{16}$$

$$\hat{\omega}^{h}_{y_{1,2}} = \omega - \Im\left(c_{\omega,1}\frac{F^{\frac{dh}{dt}}_{y_1}}{F^{h}_{y_2}} + c_{\omega,2}\frac{F^{\frac{dh}{dt}}_{y_2}}{F^{h}_{y_1}}\right). \tag{17}$$

Given $h(t) = a(-t)$ and through the use of Gauss's approximation of variance of quotients, it can be shown that the choice

$$\begin{bmatrix} c_{t,1} & c_{t,2} \end{bmatrix} = 2\frac{A_1 A_2}{A_1^2 s_2^2 + A_2^2 s_1^2}\begin{bmatrix} s_2^2 & s_1^2 \end{bmatrix},$$

is optimal to minimize the variance of (17), for t close to t_0. Note that if $s_1 = s_2$ we come back to (15). However, (17) will not be utilized in the novel multitaper phase reassignment method proposed next.

For lower variance of the final phase reassignment, we propose the averaging of reassignment vectors. The vectors in (13,14) with $h(t) = h_1(t) = a(-t)$ are averaged with the corresponding second Hermite function reassignment vectors similar to the expressions in (9,10) giving

$$\hat{t}^{h_{1,2}}_{y_{1,2}} = t + \frac{1}{2}c_t\Re\left(\frac{F^{th_1}_{y_1}}{F^{h_1}_{y_2}} + \frac{F^{th_1}_{y_2}}{F^{h_1}_{y_1}}\right) + \frac{1}{2}d_t\Re\left(\frac{F^{th_2}_{y_1}}{F^{h_2}_{y_2}} + \frac{F^{th_2}_{y_2}}{F^{h_2}_{y_1}} - \sigma^2\left(\frac{F^{\frac{dh_2}{dt}}_{y_1}}{F^{h_2}_{y_2}} + \frac{F^{\frac{dh_2}{dt}}_{y_2}}{F^{h_2}_{y_1}}\right)\right) \tag{18}$$

and

$$\hat{\omega}^{h_{1,2}}_{y_{1,2}} = \omega - \frac{1}{2}c_\omega\Im\left(\frac{F^{\frac{dh_1}{dt}}_{y_1}}{F^{h_1}_{y_2}} + \frac{F^{\frac{dh_1}{dt}}_{y_2}}{F^{h_1}_{y_1}}\right) - \frac{1}{2}d_\omega\Im\left(\frac{F^{\frac{dh_2}{dt}}_{y_1}}{F^{h_2}_{y_2}} + \frac{F^{\frac{dh_2}{dt}}_{y_2}}{F^{h_2}_{y_1}} - \frac{1}{\sigma^2}\left(\frac{F^{th_2}_{y_1}}{F^{h_2}_{y_2}} + \frac{F^{th_2}_{y_2}}{F^{h_2}_{y_1}}\right)\right). \tag{19}$$

We refer to this method as multitaper phase reassignment (MTPR) and focus on equal amplitude signals, i.e. $A_1 = A_2$, resulting in simplification of the scaling parameters to $c_t = c_\omega = 2$ and $d_t = d_\omega = 1$.

V. Simulations

Signal pairs $y_1(t)$ and $y_2(t)$ are defined by the real part of Eq. (11) and with parameters $A_1 = A_2 = 1$, $t_0 = 50$, $\omega_0 = 0.620$, and $\phi_1 = \phi_2 \in U[-\pi\ \pi]$. Independent Gaussian white noise (GWN) sequences are added to the signals, with SNR defined as the average power of the signal within $\pm 3\sigma$ of the envelope to the noise variance. An example of $y_1(t)$ is presented in Figure 1a, light blue line and with the envelope marked with a dotted green line with an example of SNR=3 dB as the dash-dotted blue line. We simulate $y_1(t)$, $t = 0 \dots 99$, and $y_2(t)$, $t = k \dots 99 + k$, where $y_2(t)$ can be shifted for values of $k = -5 \dots 5$ with $k = 0$ representing phase synchrony of the two signals in the pair. A few examples of the set representing the various shifted $y_2(t)$ are presented in Figure 1b.

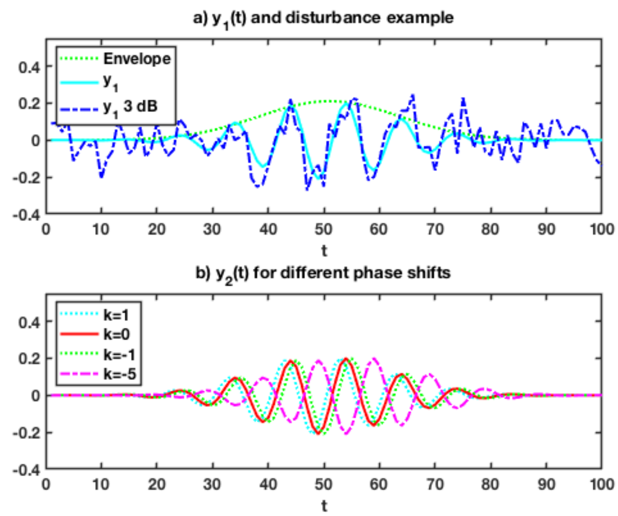

Fig. 1. a) The figure shows the transient oscillating signal (light blue line) with envelope (dotted green line), and the dash-dotted blue line shows an example of the signal in Gaussian white noise (GWN), 3 dB; b) A corresponding simulated signal $y_2(t)$ where phase synchronization with $y_1(t)$ in a) is received for $k = 0$ (red line).

We evaluate the MTPR performance and compare with the MPR and a number of state-ot-the-art estimators for their ability to detect phase synchrony at the time-shift of $k = 0$, comparing to all possible cases $k \neq 0$. For the MTPR and MPR, the Rényi entropy with $\alpha = 3$ is used as measure, where a minimum value over different values of k is taken as measure of synchronization [17]. The resulting optimal $\hat{k}_{opt}$ is compared with the same evaluation using a number of state-of-the-art phase estimators, such as the commonly applied time-based Pearson's linear correlation (CORR), time-frequency cross-spectrogram phase (XSP) [8], and Phase Lag Index (PLI) [18]. For CORR, $\hat{k}_{opt}$ is naturally the corresponding k for the largest correlation value. The cross-spectrogram of the XSP is computed using the matched Gaussian window, and the resulting phase estimate is found as the average of the extracted phases at the maximum absolute value at each time point. The PLI is calculated from the signals' Hilbert transforms and the corresponding angle differences, reconstructed into positive or negative values using the sign operator, are then finally averaged. The optimal phase estimates for XSP and PLI are the ones closest to zero.

1) Simulation 1: The simulation is repeated 1000 times for SNR ranging from 50 dB to -6 dB, and the percentage of correct estimates is defined as $|\hat{k}_{opt}| \leq 1$. The results are shown in Figure 2a, where we see that the results of MTPR, MPR and CORR have a similar performance, with 100% correct phase estimates for values larger than SNR=10 dB. For lower SNR, closer to SNR=0 dB, the MTPR outperforms the MPR and CORR, showing the value of averaged reassignment vectors in high noise levels.

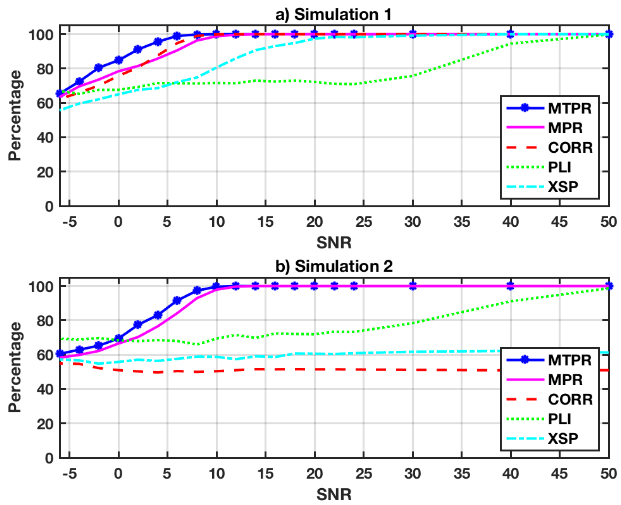

Fig. 2. Percentage of correct estimates for all methods and different SNRs; a) Simulation 1, transient oscillating signal in GWN disturbance; b) Simulation 2, transient oscillating signal in GWN disturbance and with transient disturbances $d_1(t)$ and $d_2(t)$ as defined in Eq. (20) of opposite phases.

2) Simulation 2: In simulation 2 we introduce additional transient disturbances into $y_1(t)$ and $y_2(t)$, defined by

$$d_n(t) = A_d a(t - t_d) e^{-i\omega_d t} e^{-i\phi_{dn}} \quad n = 1, 2 \tag{20}$$

where both have the same Gaussian envelopes as the actual signal, and $A_d = 1$, $t_d = 50$, $\omega_d = 1.257$. The phases are $\phi_{d1} = 1.89$ and $\phi_{d2} = 5.03$, resulting in opposite phases. The transient disturbances show up at the same time as the original signal, with the same amplitude, but the frequency is different from the signals oscillating frequency. The (local) SNR is defined similarly as before (excluding $d_n(t)$) and is evaluated over the same range as in simulation 1.

The MTPR, MPR as well as the XSP could be restricted to be evaluated locally in frequency. However, in this simulation we choose to include the whole time and frequency range of the TF spectrum of these methods to make a fair comparison between the time-based and the TF based methods. We do not use any a priori information of the transient disturbance TF location. The results are shown in Figure 2b. The results of MTPR and MPR are now superior to all the other methods due to the ability to estimate the phase synchronization correctly for all repetitions at least down to SNR=10 dB, where the MTPR gives 100% correct estimates and MPR somewhat lower. For all the other methods the degradation is severe.

VI. Electroencephalogram Example

We also compare all methods using an example of phase difference estimation of Electroencephalogram (EEG) data measured during a visual stimulation with a 9 Hz flickering light (Grass Photic stimulator Model PS22C). Data was recorded using a Neuroscan system with a digital amplifier (SYNAMP 5080, Neuro Scan, Inc.). Amplifier band-pass settings were 0.3 and 50 Hz and the sample rate was 256 Hz. The light stimulation lasted for the time interval of about 1 s so the

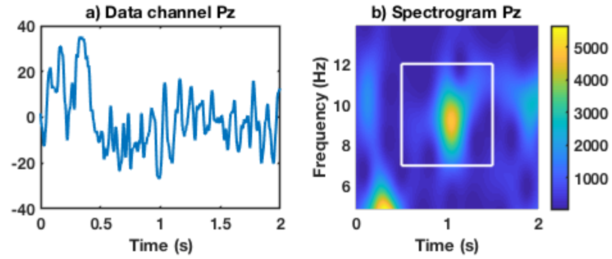

Fig. 3. a) Data measured from channel Pz; b) The corresponding spectrogram with the limits for the phase analysis marked as a white box.

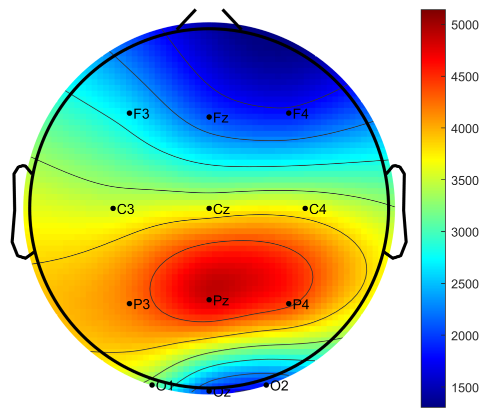

Fig. 4. The spatial distribution of the peak power for all different channels.

MTPR, MPR and XSP are all using a Gaussian window of 0.7 s, measured as the time of the range $\pm 3\sigma$. The subject had closed eyes and the flickering light was flashed at the subject from a distance of approximately 1 m. From the collected data, shorter sequences were extracted for further analysis. We focus on the time interval of the flickering light, which is starting at the time point of 0.5 s in the data example seen in Figure 3a. The corresponding spectrogram is visualized in Figure 3b where also TF limits for the phase analysis is indicated with the white box. In Figure 4 the spatial distribution of the peak power inside these limits, measured from the spectrogram, is depicted.

From the corresponding reassigned spectrogram, the time- and frequency indices of the peaks are found for all different channels, see Figure 5a and b respectively, where the channel numbers correspond to the order of the channels according to F3, Fz, F4, C3, Cz, C4, P3, Pz, P4, O1, Oz, O2. It is clearly seen that the peak location is stable between channels. For the phase difference estimation, one channel is time-shifted until the best synchronization is found, and the time-shift is used as estimate of the phase difference. All channels are compared to the occipital channel Oz, placed above the primary visual area. The frequency range is limited to 7-12 Hz using an FIR band-pass filter of length 200 applied to the measured signals used for analysis with the CORR and PLI methods. The amplitudes

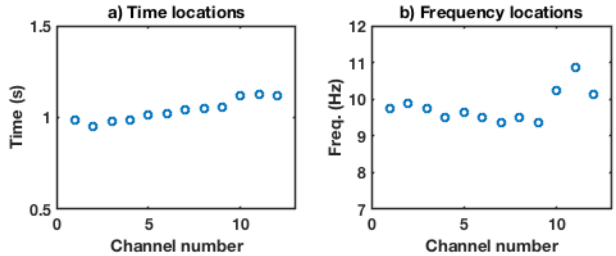

Fig. 5. a) Time locations and b) frequency locations of the reassigned spectrogram peak for all different channels ordered according to F3, Fz, F4, C3, Cz, C4, P3, Pz, P4, O1, Oz, O2.

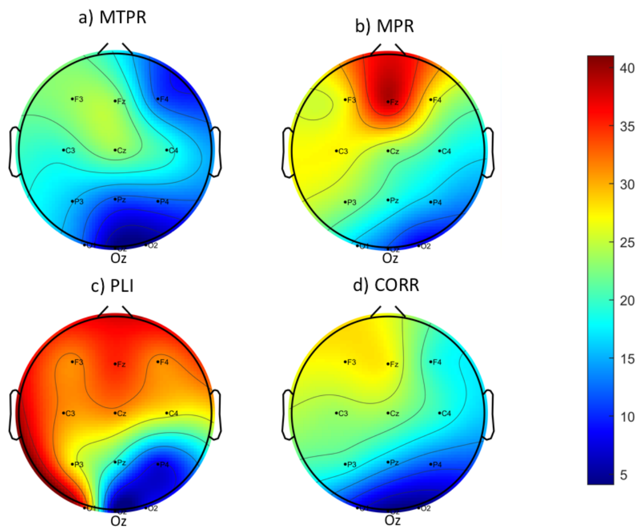

Fig. 6. The figures show the time-differences in ms of all channels compared to channel Oz (located in the middle back).

$\hat{A}_1$ and $\hat{A}_2$ are estimated from the maxima of $F^h_{y_1}(t,\omega)$ and $F^h_{y_2}(t,\omega)$ in the chosen time-frequency limits and included in Eq. (15).

A smaller phase difference should naturally be found for channels closer to Oz whereas a larger difference is expected for channels closer to the eyes. The phase pattern should also be symmetrical with respect to left and right side of the head as the origin is Oz. The results of MTPR, MPR, PLI and CORR are seen in Figure 6 with the colors representing the phase difference in ms. The results of XSP do not show the expected phase difference and is therefore not visualized. For the other methods we see the expected larger values for the frontal channels F3, Fz, and F4. For all methods, there is a small tendency for larger phase values on the left side. The MTPR, PLI and CORR all give close to zero phase difference for channel Oz. This is not the case for MPR, indicating that this method is unreliable. The estimated phase for channel Fz is also very large (39 ms) compared to the values of the other methods. Similarly we note that the phase estimate for O1 of PLI is too large (35 ms). The MTPR and CORR show similar patterns but the estimated phases of MTPR are generally 5 ms smaller than the estimated phases of CORR.

VII. Conclusions

A Multitaper Phase Reassignment (MTPR) method is proposed for robust estimation of the phase synchrony between two short oscillatory transient signals. The MTPR method is evaluated for phase estimation, by time-shifting one of the signals for the the optimal phase synchronization. The method's evaluation has shown to better estimate the phase difference with respect to other state-of-the-art methods both in simulations and in the real EEG data case.

References

[1] J.-D. Haynes and G. Rees, "Decoding mental states from brain activity in humans," *Nat Rev Neurosci*, vol. 7, pp. 523–534, 2006.

[2] A. G. Huth, W. A. de Heer, T. L. Griffiths, F. E. Theunissen, and J. L. Gallant, "Natural speech reveals the semantic maps that tile human cerebral cortex." *Nature*, vol. 532, 2016.

[3] J. Jiang, I. Bramão, A. Khazenzon, S. Wang, M. Johansson, and A. D. Wagner, "Temporal dynamics of memory-guided cognitive control and generalization of control via overlapping associative memories," *Journal of Neuroscience*, vol. 40, pp. 2343–2356, 2020.

[4] C. Kerrén, I. Bramão, R. Hellerstedt, and M. Johansson, "Strategic retrieval prevents memory interference: the temporal dynamics of retrieval-orientation," *Neuropsychologia*, 2021, 107776.

[5] I. Bramão and M. Johansson, "Neural pattern classification tracks transfer-appropriate processing in episodic memory." *eNeuro*, vol. 5, no. 4, 2018.

[6] B. He, L. Astolfi, P. A. Valdés-Sosa, D. Marinazzo, S. O. Palva, C.-G. Bénar, C. M. Michel, and T. Koenig, "Electrophysiological brain connectivity: Theory and implementation," *IEEE Trans. on Biomed. Eng.*, vol. 66, no. 7, 2019.

[7] C. M. Michel and T. Koenig, "EEG microstates as a tool for studying the temporal dynamics of whole-brain neuronal networks: A review." *NeuroImage*, vol. 180, no. Part B, pp. 577–593, 2018.

[8] L. Cohen, *Time-Frequency Analysis*, ser. Signal Processing Series. Upper Saddle River, NJ, USA: Prentice-Hall, 1995.

[9] F. Auger and P. Flandrin, "Improving the readability of time-frequency and time-scale representations by the reassignment method," *IEEE Trans. on Signal Processing*, vol. 43, pp. 1068–1089, May 1995.

[10] M. Hansson-Sandsten and J. Brynolfsson, "The scaled reassigned spectrogram with perfect localization for estimation of Gaussian functions," *IEEE Signal Processing Letters*, vol. 22, no. 1, pp. 100–104, 2015.

[11] M. Sandsten, J. Brynolfsson, and I. Reinhold, "The matched window reassignment," in *EUSIPCO*, Rome, Italy, 2018.

[12] J. Brynolfsson and M. Sandsten, "Parameter estimation of oscillating Gaussian functions using the scaled reassigned spectrogram," *Signal Processing*, vol. 150, pp. 20–32, 2018.

[13] J. Brynolfsson, I. Reinhold, and M. Sandsten, "A time-frequency-shift invariant parameter estimator for oscillating transient functions using the matched window reassignment," *Signal Processing*, vol. 183, 2021, 107913.

[14] M. Sandsten, R. Anderson, I. Reinhold, and J. Brynolfsson, "The matched reassigned cross-spectrogram for phase estimation," in *Proceedings of the ICASSP*. Barcelona, Spain: IEEE, 2020.

[15] I. Daubechies, "Time-frequency localization operators: A geometric phase space approach," *IEEE Trans. on Information Theory*, vol. 34, no. 4, pp. 605–612, 1988.

[16] M. Sandsten, I. Reinhold, and R. Anderson, "A multitaper reassigned spectrogram for increased time-frequency localization precision," in *Proceedings of the ICASSP*. Barcelona, Spain: IEEE, 2020.

[17] R. G. Baraniuk, P. Flandrin, A. J. E. M. Janssen, and O. J. J. Michel, "Measuring time-frequency information content using Rényi entropies," *IEEE Trans. on Information Theory*, vol. 47, no. 4, pp. 1391–1409, May 2001.

[18] C. J. Stam, G. Nolte, and A. Daffertshofer, "Phase lag index: Assessment of functional connectivity from multi channel EEG and MEG with diminished bias from common sources." *Human Brain Mapping*, vol. 28, no. 11, pp. 1178–1193, 2007.